Copyright ©2010 by Jeannette Heiligers. Published by the IAF, with permission and released to the IAF to publish in all forms.

IAC-10-E2.1.2

DISPLACED GEOSTATIONARY ORBITS USING HYBRID LOW-THRUST PROPULSION

Jeannette Heiligers
Advanced Space Concepts Laboratory, University of Strathclyde, Glasgow, United Kingdom
Jeannette.Heiligers@strath.ac.uk

In this paper, displaced geostationary orbits using hybrid low-thrust propulsion, a complementary combination of Solar Electric Propulsion (SEP) and solar sailing, are investigated to increase the capacity of the geostationary ring that is starting to get congested. The SEP propellant consumption is minimized in order to maximize the mission lifetime by deriving semi-analytical formulae for the optimal steering laws for the SEP and solar sail accelerations. By considering the spacecraft mass budget, the performance is also expressed in terms of payload mass capacity. The analyses are performed for both the use of SEP and hybrid sail control to allow for a comparison. It is found that hybrid sail control outperforms the pure SEP case both in terms of payload capacity and mission lifetime for all displacements considered. Hybrid sails enable payloads of 250-450 kg to be maintained in a 35 km displaced orbit for 10-15 years. Finally, two transfers that allow for an improvement in the performance of hybrid sail control are optimized for the SEP propellant consumption by solving an optimal control problem using a direct pseudo-spectral method. The first type of transfer enables a transit between orbits displaced above and below the equatorial plane, while the second type of transfer enables 'customized service' in which the spacecraft is transferred to a Keplerian parking orbit when coverage is not needed. While the latter requires a modest propellant budget, the first type of transfer comes at the cost of a negligible SEP propellant consumption.

I. INTRODUCTION

Since the first geostationary spacecraft was launched in 1964, Syncom-3, hundreds of communication and weather satellites have exploited the unique properties of the geostationary orbit (GEO). With a period equal to the Earth's rotational period, GEO spacecraft are stationary with respect to their ground station, allowing for a continuous downlink to Earth. However, with only one such unique orbit, the geostationary orbit has started to get congested over time. Ref. [1] reports the status of the geostationary orbit in January 2009 and clearly shows its congestion, especially above the continents.

In order to increase the capacity of the geostationary orbit, this paper investigates the use of displaced non-Keplerian orbits (NKO). By applying a continuous acceleration to counterbalance the gravitational acceleration, the geostationary orbit can be levitated above or below the equatorial plane, thereby creating new geostationary slots [2]. The existence, stability and control of displaced NKOs have been studied for both the two- and three-body problem [3-4] and numerous applications have been proposed. The two-body problem applications include spacecraft proximity operations [5] and hovering above Saturn's rings for in-situ observations [6]. NKOs displaced high above the ecliptic have been proposed in the Earth-Sun three-body problem to enable imaging and communication satellites for high latitudes [7], while displaced NKOs in the Earth-Moon system have been studied for lunar far side communication and lunar south pole coverage [8-9].

Solar sails have often been proposed as spacecraft propulsion system to maintain displaced NKOs [2, 4, 7-8, 10]. Solar sails exploit the radiation pressure generated by photons reflecting off a large, highly reflecting sail to produce a continuous, propellant-less thrust [2]. This makes them seemingly suitable to maintain displaced NKOs. However, only recently the use of solar sail technology was successfully demonstrated in space by the Japanese IKAROS spacecraft [11]. This low Technology Readiness Level (TRL) in combination with a high Advanced Degree of Difficulty (AD^2) and the inability to generate a thrust component in the direction of the Sun pose severe limits on its applications and put many solar sail applications in the far-future [2, 12]. Solar sails have also been proposed to make levitated geostationary orbits possible [13]. However only small displacements, still inside the geostationary station keeping box, appeared to be feasible and a residual in-plane sail acceleration caused the spacecraft to move with respect to its ground station.

Copyright ©2010 by Jeannette Heiligers. Published by the IAF, with permission and released to the IAF to publish in all forms.

Solar Electric Propulsion (SEP) has also been considered as a means to maintain displaced NKOs [9, 14]. SEP is highly efficient as it enables high specific impulses. It has flown on multiple missions including Deep Space 1 (1998), SMART-1 (2003) Dawn (2007) and GOCE (2009) resulting in a high TRL and a low AD^2 [15-17]. Nevertheless, the applications of SEP are limited due to a bound on the available propellant mass.

Considering the advantages and disadvantages of solar sails and SEP, some authors are suggesting the use of hybrid sails, a complementing combination of a solar sail and an SEP system. While the solar sail lowers the demand on the SEP propellant mass, the SEP system can provide the thrust component in the direction of the Sun that the solar sail cannot generate and lower the solar sail AD^2 as only small solar sails are required. Hybrid sails have been suggested to enable interplanetary transfers [18-19], to allow for periodic orbits in the vicinity of the Lagrange points in the Earth-Moon system for lunar communication purposes [20], and to generate artificial equilibria in the Earth-Sun three-body problem [21], for instance for an Earth-Mars communications relay during periods of solar occultation [22] and to enable an Earth pole-sitter [23]. All studies show to some extent an improvement for hybrid sails in terms of propellant mass consumption, required thrust magnitude levels and/or initial spacecraft mass over the use of pure SEP or pure solar sailing.

In this paper we propose the use of hybrid sails to enable displaced geostationary orbits. This will allow spacecraft to be stationary with respect to their ground station and enable displacements well beyond the geostationary station keeping box, using relatively small, near-term solar sails. The objective is to minimize the propellant consumption, thereby either decreasing launch mass, increasing payload mass or increasing the mission lifetime. To assess the performance of hybrid sail control, its results are compared with results for the use of pure SEP control. Finally, the optimization of two transfers that improve the performance of hybrid sail control will be considered: a transfer between orbits displaced above and below the equatorial plane and a transfer between the displaced orbit and a Keplerian parking orbit to enable 'customized service'.

The structure of the paper is as follows. First the general theory underlying displaced geostationary orbits will be presented. Subsequently the performance of SEP and hybrid sail control in terms of propellant consumption will be derived and a comparison between the two control strategies will be made. A mass budget analysis will subsequently consider the performance of both types of control in terms of payload mass. Finally, the analysis to optimize the two transfers to improve the performance of hybrid sail control will be outlined and the results will be presented.

II. DISPLACED GEOSTATIONARY ORBITS

Displaced geostationary orbits, or displaced NKOs in general, can be found by seeking equilibrium solutions to the two- or three-body problem in a rotating frame of reference. A transformation to an inertial frame will subsequently show that the spacecraft executes a circular orbit displaced away from the centre of the central body [3]. The situation as it occurs in the displaced geostationary orbit is depicted in Fig. 1, indicating the rotating reference frame $R(x_R, y_R, z_R)$ that rotates with constant angular velocity $\boldsymbol{\omega} = \omega \hat{\mathbf{z}}_R$ with respect to an inertial frame $I(X, Y, Z)$. The figure shows that the geostationary orbit is levitated over a distance h while keeping both the orbital radius and the orbital angular velocity equal to the orbital radius and orbital angular velocity in the geostationary orbit, r_{GEO} and ω respectively, causing spacecraft in the (displaced) geostationary orbit to be stationary in the rotating frame. This case corresponds to a 'Type I' NKO for which the thrust induced acceleration required to maintain the NKO is at its minimum for a given radius of the NKO and which is stable for modest displacements [2]. Following the analysis in Ref. [2], the required direction, $\hat{\mathbf{n}}$ (see Fig. 1), and magnitude, a, of this acceleration are:

$$\tan\alpha = 0$$
$$a = h\omega^2 = \frac{\mu h}{r_{GEO}^3} \qquad (1)$$

with μ the gravitational parameter of the Earth. Eq. (1) shows that a thrust perpendicular to the displaced geostationary orbit is required and that the magnitude of the thrust is merely a function of the gravitational parameter, the displacement distance and the orbital radius. Note that for a geostationary orbit displaced above the equatorial plane ($h > 0$) the required acceleration is directed in positive Z-direction, while for orbits displaced below the equatorial plane ($h < 0$) the acceleration is directed in negative Z-direction.

With the gravitational parameter and the orbital radius given, the only parameter that needs to be specified is the displacement distance. While the displacement should be as small as possible to minimize the required acceleration, it should be large enough to prevent the spacecraft from interfering with other satellites in the geostationary orbit. To prevent radio frequency interference and collisions the International Telecommunication Union (ITU) states that geostationary spacecraft should be maintained within 0.1° longitude and latitude of their nominal position. Some individual countries have specified even stricter station keeping regulations. For example, the US

Copyright ©2010 by Jeannette Heiligers. Published by the IAF, with permission and released to the IAF to publish in all forms.

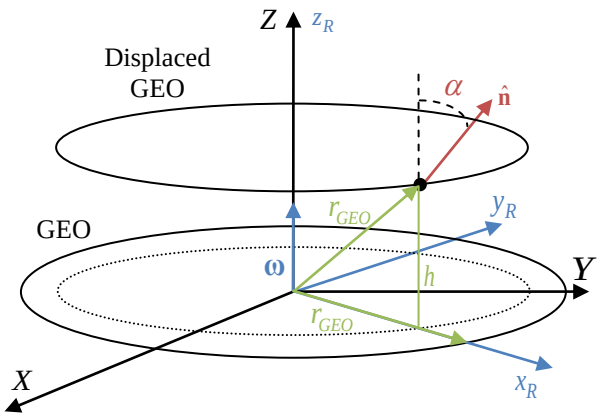

Fig. 1: Definition of displaced geostationary orbit (GEO)

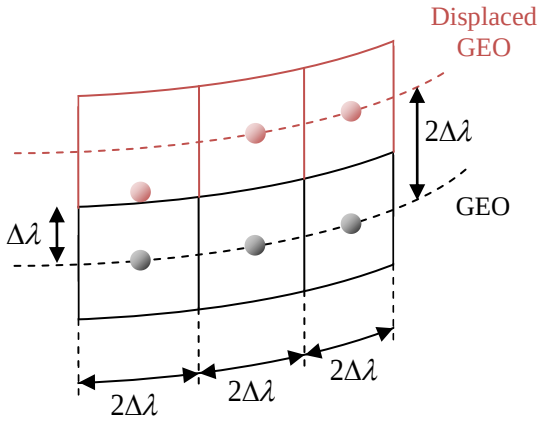

Fig. 2: Definition of geostationary station keeping box

Federal Communications Commission (FCC) requires that geostationary spacecraft should be maintained within 0.05° of their assigned location [24-25]. From Fig. 2, these regulations lead to a geostationary station keeping box of $2\Delta\lambda = 0.1^\circ - 0.2^\circ$ equalling 73.6 – 147.2 km. Since the displaced geostationary spacecraft will be an actively controlled satellite, one could argue that the displacement distance would only have to be $\Delta\lambda$. However, to ensure a similar station keeping box for the displaced spacecraft as for geostationary spacecraft, the displacement distance might have to be increased to $2\Delta\lambda$, leading to a range for the displacement distance of 36.8 – 147.2 km. This paper will therefore consider three different displacement distances, namely 35, 75 and 150 km both above and below the equatorial plane.

III. SOLAR ELECTRIC PROPULSION

This section investigates the use of SEP to provide the continuous acceleration required to maintain the displaced geostationary orbit. Its performance in terms of propellant consumption can be assessed by integrating the following differential equation for the mass:

$$\dot{m} = -\frac{T}{I_{sp} g_0} \tag{2}$$

with T the SEP thrust magnitude, I_{sp} the SEP system specific impulse and g_0 the Earth gravity constant (9.80665 m/s^2). The lifetime of the mission, L, is subsequently defined as the epoch at which a particular mass fraction m_f / m_0 is obtained, with

$$m_f / m_0 = \left(m_0 - m_{prop}\right) / m_0 \tag{3}$$

m_0 is the initial mass, m_f the final mass (i.e. the mass at lifetime L) and m_{prop} is the propellant mass. The lifetime can be derived analytically from Eq. (2) as the required acceleration is constant. Substituting $T = a \cdot m$ into Eq. (2) with a given by Eq. (1) and rearranging gives:

$$\int_{m_0}^{m_f} \frac{dm}{m} = -\int_{t_0}^{t_f} \frac{a}{I_{sp} g_0} dt \tag{4}$$

Evaluating these integrals and setting $t_0 = 0$ yields the following lifetime for a particular mass fraction:

$$L = t_f = -\ln\left(\frac{m_f}{m_0}\right) \frac{I_{sp} g_0}{a} \tag{5}$$

Fig. 3 shows the lifetimes for the three displacement distances determined in Section II and for a wide range of mass fractions and specific impulses (from current to near term and far-future technology). An arbitrary value for the initial mass can be assumed. Note that due to the symmetry of the problem, the results for orbits displaced above and below the equatorial plane are exactly the same and that only lifetimes up to 15 years are considered. Fig. 3 shows that, for example, for a 35 km displaced geostationary orbit, a currently feasible specific impulse of 3200 s (e.g. as flown on the Hayabusa spacecraft [26]) and a mass fraction of 0.5 a lifetime of 3.5 years can be achieved. However, this lifetime degrades to 1.7 and 0.9 years when considering the larger displacements of 75 and 150 km, respectively. Considering a lifetime of 10-15 years for current geostationary spacecraft, Fig. 3 shows that similar lifetimes can only be achieved for the smallest displacement of 35 km and either for low mass fractions (e.g. $m_f = 0.1$ and $I_{sp} = 3500$) or for far-future specific impulses (e.g. $m_f = 0.45$ and $I_{sp} = 8000$).

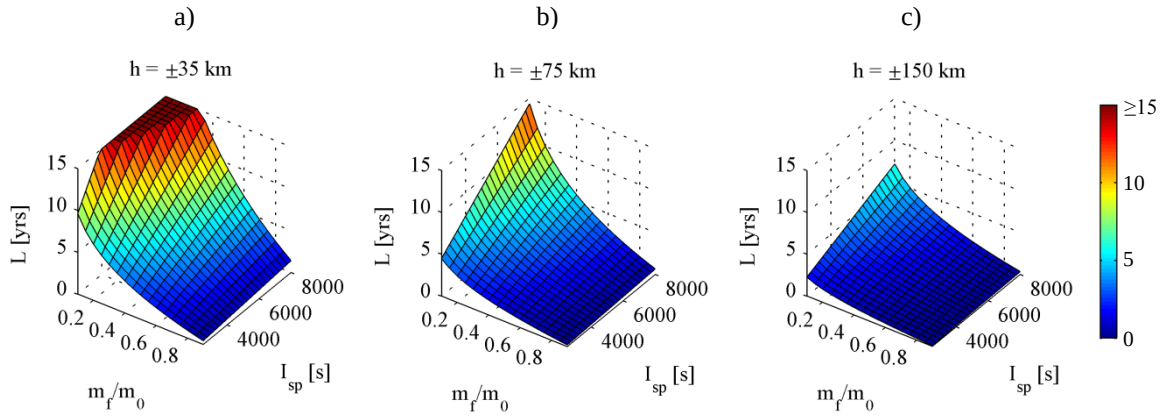

Fig. 3: Displaced geostationary orbits maintained with SEP control: mission time L as a function of the specific impulse I_{sp} and the mass fraction m_f / m_0, for different values of the displacement distance h

IV HYBRID LOW-THRUST PROPULSION

To improve the performance of SEP control in terms of propellant consumption, this section will investigate the use of hybrid sail control to maintain the displaced geostationary orbit. To assess the performance of hybrid sail control, the equations of motion for a spacecraft in the displaced geostationary orbit are derived using the rotating reference frame given in Fig. 1:

$$\ddot{\mathbf{r}} + 2\boldsymbol{\omega} \times \dot{\mathbf{r}} + \nabla U = \mathbf{a} \tag{6}$$

with $\mathbf{r}$ the position vector, $\mathbf{r} = \begin{bmatrix} x_R & y_R & z_R \end{bmatrix}^T$, U a potential that combines the gravitational potential of the central body and a potential representing the centripetal acceleration and $\mathbf{a}$ the acceleration required to obtain an equilibrium solution in the rotating frame of reference. This acceleration can be written as the sum of the acceleration generated by the SEP system, $\mathbf{a}_{SEP}$, and the acceleration produced by the solar sail, $\mathbf{a}_S$:

$$\mathbf{a} = \mathbf{a}_{SEP} + \mathbf{a}_S \tag{7}$$

To maximize the lifetime of the spacecraft, the objective is to minimize the magnitude of the acceleration required from the SEP system, thereby minimizing the propellant consumption:

$$\min\left(a_{SEP}\right) = \min\left(\left\|\mathbf{a} - \mathbf{a}_S\right\|\right) \tag{8}$$

The required acceleration is given through Eq. (1), while the acceleration generated by an ideal (i.e. a perfectly reflecting) solar sail is given by:

$$\mathbf{a}_S = \beta \frac{\mu_S}{r_S^2} \left(\hat{\mathbf{n}} \cdot \hat{\mathbf{r}}_S\right)^2 \hat{\mathbf{n}} \tag{9}$$

μ_S is the gravitational parameter of the Sun, $\mathbf{r}_S$ is the Sun-sail vector (the magnitude of the Sun-sail vector is approximated by a constant Sun-Earth distance of 1 Astronomical Unit) and $\hat{\mathbf{n}}$ is the unit vector in the direction of the solar radiation pressure force. Note that for a perfectly reflecting solar sail as considered here, $\hat{\mathbf{n}}$ is directed normal to the sail surface. Finally, β is the solar sail lightness number and can be defined as:

$$\beta = \frac{\sigma^*}{\sigma} \tag{10}$$

with σ the system loading (i.e. the ratio of the spacecraft mass to the solar sail area, $\sigma = m/A$) and σ^* the critical sail loading, a constant equal to 1.53 g/m^2 [2]. Equation (10) shows that the sail lightness number is a function of the spacecraft mass. Since the mass of the hybrid sail will decrease due to the consumption of propellant by the SEP system, the parameter β increases according to:

$$\beta = \beta_0 \frac{m_0}{m} \tag{11}$$

with β_0 and m_0 the sail lightness number and spacecraft mass at time $t = 0$.

Due to the tilt of the Earth's rotational axis with respect to the ecliptic plane, the direction of the Sun-sail vector $\mathbf{r}_S$ changes during the year. To model this variation, an Earth fixed rotating reference frame $E(x_E, y_E, z_E)$ as shown in Fig. 4 is used. Centred at the Earth with the (x_E, y_E)-plane in the equatorial plane and the z_E-axis along the rotational axis of the Earth, this reference frame rotates with the same angular velocity as the orbit of the Earth, causing the unit vector $\hat{\mathbf{r}}_S$ to always be contained in the (x_E, z_E)-plane. The angle ϕ describes the time during the year (with $\phi = 0$ at winter), while the angle ψ is defined as the angle between $\hat{\mathbf{r}}_S$ and the equatorial plane as a function of ϕ.

Copyright ©2010 by Jeannette Heiligers. Published by the IAF, with permission and released to the IAF to publish in all forms.

This angle is at its maximum in winter ($\psi(0) = i_{obl}$) and at its minimum in summer ($\psi(\pi) = -i_{obl}$) with i_{obl} the obliquity of the ecliptic. The variation of ψ is therefore in magnitude equal to the solar declination, but is opposite in sign:

$$\psi(\phi) = \sin^{-1}\left(\sin i_{obl} \cos\phi\right) \tag{12}$$

Using this definition for ψ , $\hat{\mathbf{r}}_S$ is given by:

$$\hat{\mathbf{r}}_S = \begin{pmatrix} \cos\psi \\ 0 \\ \sin\psi \end{pmatrix} \tag{13}$$

The unit vector normal to the sail surface, $\hat{\mathbf{n}}$, can be described using the same frame of reference only centred at the displaced geostationary orbit, see Fig. 5. Using the pitch angle α_S and the yaw angle δ_S , yields:

$$\hat{\mathbf{n}} = \begin{pmatrix} \sin\alpha_S \sin\delta_S \\ \sin\alpha_S \cos\delta_S \\ \cos\alpha_S \end{pmatrix} \tag{14}$$

Substituting Eq. (1) and the expressions for $\hat{\mathbf{r}}_S$, $\hat{\mathbf{n}}$ and β into Eq. (7) and rearranging gives:

$$\begin{aligned} a_{SEP,x_E} &= -\beta_0 \frac{m_0}{m}\frac{\mu_S}{{r_S}^2}(\cos\psi \sin\alpha_S \sin\delta_S + \\ &\quad \sin\psi \cos\alpha_S)^2 \sin\alpha_S \sin\delta_S \\ a_{SEP,y_E} &= -\beta_0 \frac{m_0}{m}\frac{\mu_S}{{r_S}^2}(\cos\psi \sin\alpha_S \sin\delta_S + \\ &\quad \sin\psi \cos\alpha_S)^2 \sin\alpha_S \cos\delta_S \\ a_{SEP,z_E} &= \frac{\mu h}{r_{GEO}^3} - \beta_0 \frac{m_0}{m}\frac{\mu_S}{{r_S}^2}(\cos\psi \sin\alpha_S \sin\delta_S + \\ &\quad \sin\psi \cos\alpha_S)^2 \cos\alpha_S \end{aligned} \tag{15}$$

The SEP system thus needs to counterbalance the in-plane component of the solar sail acceleration and needs to augment the out-of-plane solar sail acceleration to obtain the required out-of-plane acceleration. Eq. (8) subsequently becomes:

$$\min\left(a_{SEP}\right) = \min\left(\sqrt{{a_{SEP,x_E}}^2 + {a_{SEP,y_E}}^2 + {a_{SEP,z_E}}^2}\right) \tag{16}$$

Inspecting Eq. (15) and (16) shows that for a given value for m and ψ (i.e. for a particular instant of time), the minimization problem in Eq. (16) is merely a function of the solar sail pitch and yaw angles and therefore reduces to finding the optimal solar sail pitch and yaw angles that minimize the acceleration required from the SEP system:

$$\left({\alpha_S}^*, {\delta_S}^*\right) = \arg\min\left(a_{SEP}(\alpha_S, \delta_S)\right) \tag{17}$$

The solution to Eq. (17) can be found by setting the partial derivative of the SEP acceleration with respect to the sail pitch and yaw angles equal to zero:

$$\frac{\partial a_{SEP}}{\partial \alpha_S} = \frac{\partial a_{SEP}}{\partial \delta_S} = 0 \tag{18}$$

Performing this analysis for the yaw angle yields:

$$\begin{aligned} \frac{\partial a_{SEP}}{\partial \delta_S} &= 4c_1\left(\hat{\mathbf{n}}\cdot\hat{\mathbf{r}}_S\right)\left(c_1\left(\hat{\mathbf{n}}\cdot\hat{\mathbf{r}}_S\right)^2 - c_2\cos\alpha_S\right)\cdot \\ &\quad \cos\psi \sin\alpha_S \cos\delta_S = 0 \end{aligned} \tag{19}$$

with

$$c_1 = \beta_0 \frac{m_0}{m}\frac{\mu_S}{{r_S}^2}, \quad c_2 = \frac{\mu h}{r_{GEO}^3} \tag{20}$$

For Eq. (19) to hold throughout the year and considering that $c_1 \neq 0$ and $(\hat{\mathbf{n}}\cdot\hat{\mathbf{r}}_S) > 0$ (to generate a

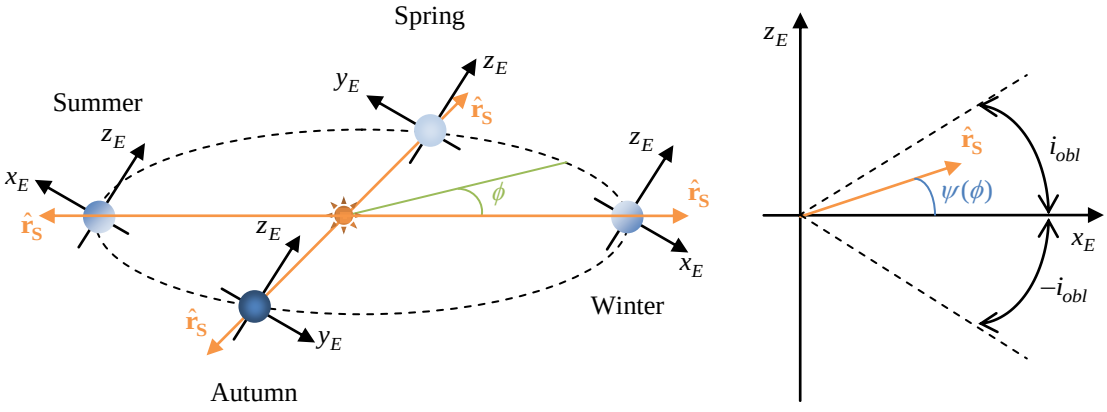

Fig. 4: Definition of reference frame and parameters used to model the seasonal variation of $\hat{\mathbf{r}}_S$

Copyright ©2010 by Jeannette Heiligers. Published by the IAF, with permission and released to the IAF to publish in all forms.

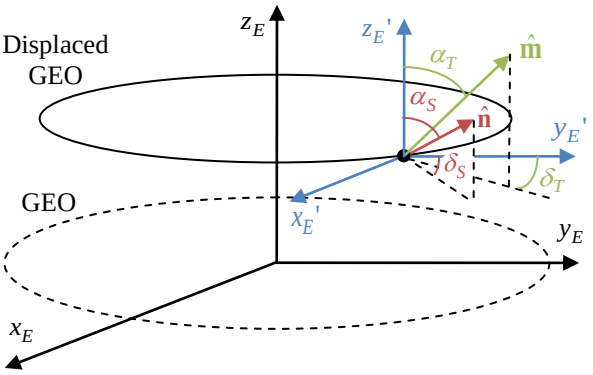

Fig. 5: Definition of solar sail and SEP pitch and yaw angles

solar sail acceleration) the optimal yaw angle equals:

$$\delta_S^* = \pm\pi/2 \tag{21}$$

Substituting this value into Eq. (15) shows that the y_E-component of the SEP thrust force is zero at all times. Considering the fact that the solar sail is unable to generate a thrust component in the direction of the Sun and recalling that the x_E-axis points away from the Sun at all times, Eq. (21) can be reduced to:

$$\delta_S^* = \pi/2 \tag{22}$$

This reduction also guarantees that $\partial^2 a_{SEP} / \partial \delta_S{}^2 > 0$ such that the solution corresponds to a minimum rather than a maximum of $a_{SEP}(\alpha_S, \delta_S)$. A similar analysis can be performed for the partial derivative with respect to the sail pitch angle. Immediately substituting $\delta_S = \delta_S^* = \pi/2$ gives:

$$\frac{\partial a_{SEP}}{\partial \alpha_S} = \sin(\alpha_S + \psi) - \frac{c_2}{c_1}\frac{\cos\alpha_S}{\sin(\alpha_S+\psi)} + \frac{c_2}{2c_1}\frac{\sin\alpha_S}{\cos(\alpha_S+\psi)} = 0 \tag{23}$$

The optimal pitch angle cannot be retrieved analytically from this expression. A numerical method such as Newton's method (e.g. see Ref. [27]) will have to be applied to find α_S^*. To ensure that the optimal pitch angle does not generate a normal vector $\hat{\mathbf{n}}$ pointing towards the Sun, bounds are imposed on the optimum pitch angle. These bounds are a function of the angle ψ as is shown in Fig. 6 for three epochs during the year:

$$\begin{aligned} \alpha_{S,\min} &= -\psi \\ \alpha_{S,\max} &= \pi - \psi \end{aligned} \tag{24}$$

Then, to ensure $\partial^2 a_{SEP} / \partial \alpha_S{}^2 > 0$, these bounds are set even tighter depending on whether a displacement above or below the equator is considered:

$h > 0$:	$h < 0$:
$\alpha_{S,\min} = -\psi$	$\alpha_{S,\min} = 0.5\pi$
$\alpha_{S,\max} = 0.5\pi$	$\alpha_{S,\max} = \pi - \psi$

Note that Fig. 6 clearly illustrates that the displaced geostationary orbit as presented in this paper cannot be maintained throughout the year using only solar sailing. For instance, in summer the shaded half-circle shows that the required thrust direction for a displaced geostationary orbit displaced *above* the equatorial plane (i.e. a thrust along the positive z_E-axis) cannot be

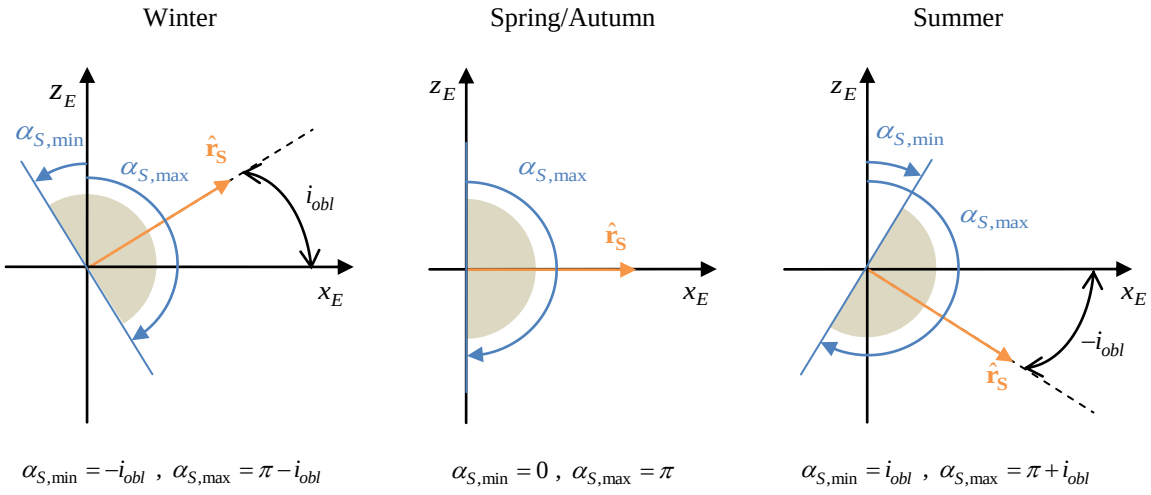

Fig. 6: Definition of minimum and maximum solar sail pitch angles during the year

Copyright ©2010 by Jeannette Heiligers. Published by the IAF, with permission and released to the IAF to publish in all forms.

achieved by the solar sail. A similar reasoning holds for a geostationary orbit displaced *below* the equatorial plane in winter. Furthermore, in autumn and spring the required thrust direction for orbits displaced both above and below the equator lies on the edge of the shaded half-circle. The magnitude of the solar sail acceleration along the z_E - axis in that case becomes equal to zero as the Sun shines edge-on to the solar sail. This result also follows from substituting $\phi = \pm\pi/2$ into Eq. (12), and subsequently evaluating Eq. (13) and (9). In all these cases, a solar sail acceleration along the z_E -axis can only be achieved by tilting the normal vector $\hat{\mathbf{n}}$ away from the z_E -axis resulting in an acceleration component parallel to the equatorial plane, which has to be cancelled out by some other means such as an SEP system.

Once the optimal sail pitch and yaw angles are found, the magnitude and direction, $\hat{\mathbf{m}}$, of the required SEP acceleration can be computed. Note that the assumption is made that the solar sail and SEP system can steer independently of each other. Using Eq. (15) and the notation in Fig. 5, the pitch and yaw angles of the SEP acceleration can be computed:

$$\begin{aligned} \alpha_T &= \cos^{-1}\left(\frac{a_{SEP,z}}{a_{SEP}}\right) \\ \delta_T &= \cos^{-1}\left(\frac{a_{SEP,y}/a_{SEP}}{\sin\alpha_T}\right)\mathrm{sgn}\left(a_{SEP,x}\right) \end{aligned} \tag{25}$$

as well as the magnitude of the required SEP thrust force:

$$T = m \cdot a_{SEP} \tag{26}$$

Previously it was already stated that $a_{SEP,y_E} = 0$ since $\delta_S^* = \pi/2$. Substituting this known into Eq. (25) gives $\delta_T = \pm\pi/2$.

As mentioned before, the above holds for one instant in time, i.e. for a given value for m and ψ. To find the variation of the controls, accelerations, thrust magnitude and mass as a function of time over multiple orbital periods, the displaced geostationary orbit is discretized into several nodes. When the node spacing is chosen small enough, a fair comparison with the analytical analysis in Section III can be made. The nodes are equally distributed over the orbit, leading to a constant time interval Δt in between two consecutive nodes. At each node, i, the required SEP thrust magnitude can be approximated using Eq. (26):

$$T_i = m_i \cdot a_{SEP} \tag{27}$$

Assuming a constant thrust magnitude during the interval Δt, the mass at the end of the i^{th} interval can be approximated through:

$$m_{i+1} = m_i - \frac{T_i}{I_{sp} g_0}\Delta t \tag{28}$$

At each node the optimum solar sail angles (and subsequently the SEP acceleration, thrust magnitude and thrust angles) can be computed. When changing from one node to the successive node, the change in ψ is computed using Eq. (12), while the mass at the start of the new interval is given by Eq. (28).

The results after one year in a geostationary orbit displaced 35 km along the positive z_E -axis are shown by the solid lines in Fig. 7. A time interval of $\Delta t = 0.005 t_{day}$ (with t_{day} the length of a day) is adopted together with an initial mass of 1500 kg (the smaller class of geostationary spacecraft [28]) and a specific impulse of 3200 s. Four different values for the sail lightness number are used, $\beta_0 = 0.01$, 0.05, 0.1 and 0.2. Some discontinuities can be observed in the profiles of the SEP thrust angles for the largest value of β_0, which can be explained by the slightly negative value for the solar sail pitch angle and the large value for β_0. The negative value for α_S (which is allowed because it is winter time, see Fig. 6) produces a component of the solar sail acceleration along the negative x_E -axis. Because the SEP system has to counterbalance this acceleration, the yaw angle needs to switch from the 'usual' $\delta_T = -\pi/2$ to $\delta_T = \pi/2$. Furthermore, the large value of β_0 causes the component of the solar sail acceleration along the positive z_E -axis to become larger than the required out-of-plane acceleration. This requires the SEP thruster to thrust along the negative z_E -axis to counterbalance the access out-of-plane acceleration. Hence, the switch in the SEP pitch angle from $\alpha_T < \pi/2$ to $\alpha_T > \pi/2$.

Fig. 7b furthermore shows the expected lower demand on the SEP system by using hybrid sail control which is directly translated into a larger final mass after 1 year in-orbit. Already a small solar sail with β_0 = 0.01 provides a gain of 29 kg. Increasing β_0 results in savings of 94, 130 and 161 kg for β_0 = 0.05, 0.1 and 0.2, respectively.

Finally, looking at the required thrust magnitude in Fig. 7c, another great advantage of hybrid sails over SEP becomes evident as hybrid sails lower the required SEP thrust magnitude. Currently feasible maximum thrust levels are in the order of 0.2 N at maximum power (e.g. EADS/Astrium RIT-XT). While the

Copyright ©2010 by Jeannette Heiligers. Published by the IAF, with permission and released to the IAF to publish in all forms.

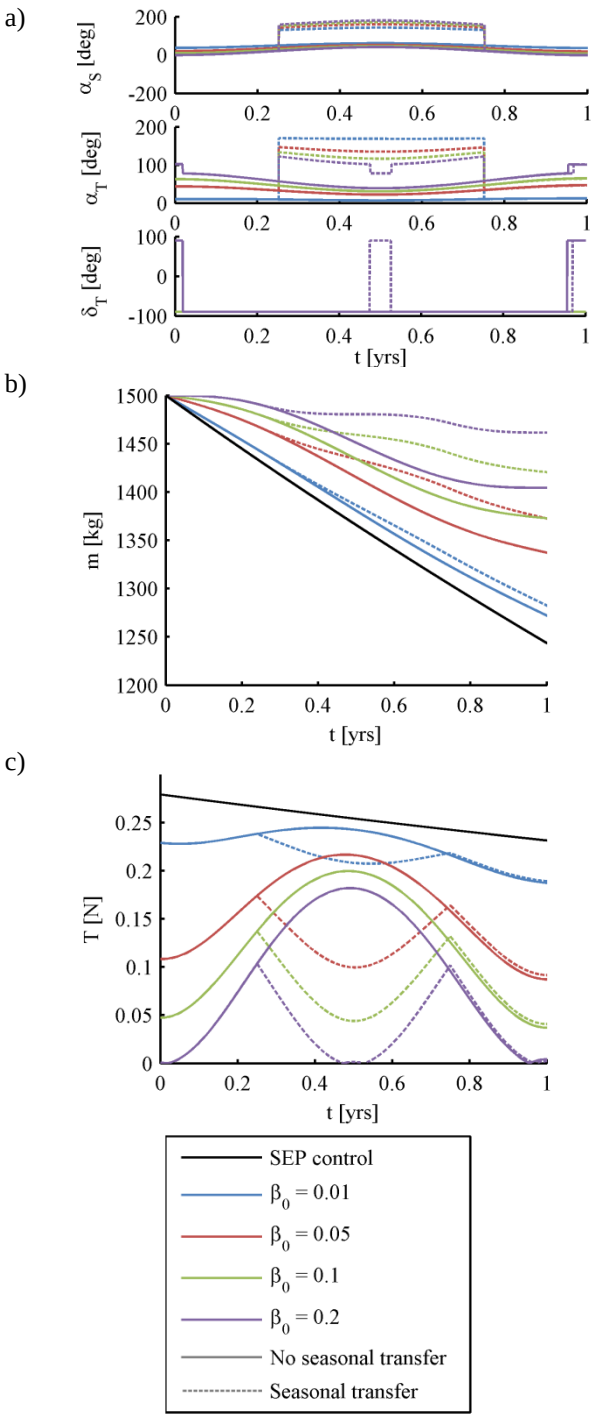

Fig. 7: 35 km displaced geostationary orbit maintained with hybrid sail control with different values for the solar sail lightness number β_0. Solid lines indicate a year-long displacement along the positive z_E-axis. Dotted lines include a 'seasonal transfer'. a) Optimal solar sail pitch angle and SEP pitch and yaw angles. b) Spacecraft mass assuming an initial mass of 1500 kg and a specific impulse of 3200 s. c) Required SEP thrust magnitude.

thrust level required for a 1500 kg spacecraft with SEP control exceeds this value, thrust levels smaller than 0.2 N throughout the year can be observed for β_0 = 0.1 and 0.2. Even for β_0 = 0.05 the thrust level remains well under 0.2 N during winter, but is unfortunately too high during summer. This performance can be improved by transferring the spacecraft from a geostationary orbit displaced above the equatorial plane to an orbit displaced below the equatorial plane before summer. Then, the performance of the sail is no longer limited by the unfavourable obliquity of the ecliptic and can perform equally well in summer as it does in winter above the equatorial plane. When this so-called 'seasonal transfer' is introduced in the model, results as presented by the dotted lines in Fig. 7 are obtained. Note that the mission is assumed to always start in winter, i.e. above the equatorial plane. As can be expected, massive improvements both in terms of propellant consumption and required thrust levels can be observed. The mass savings mentioned before are now increased to 39, 129, 178 and 219 kg for β_0 = 0.01, 0.05, 0.1 and 0.2, respectively. Section VI of this paper will show that transfers from above to below the equatorial plane and vice versa are possible and come at the cost of an almost negligible SEP propellant consumption.

While the results in Fig. 7 only hold for a mission of 1 year, it is interesting to investigate whether hybrid propulsion can enable missions lasting as long as current geostationary missions. Fig. 3 already showed that SEP control is unable to do so. Extending the mission lifetime for hybrid sail control results in the graphs shown in Fig. 8 which include the 'seasonal transfer' to optimize the displaced geostationary orbit to its fullest and use an arbitrary initial mass. Again, the three displacement distances of Section II are considered. The notation h_0 is used rather than h to indicate that the spacecraft starts at a particular displacement (always above the equatorial plane for the results in Fig. 8) but is transferred between displacements above and below the equatorial plane during its lifetime.

Comparing Fig. 3 with Fig. 8 shows a dramatic improvement of the lifetime for hybrid sail control compared to pure SEP control. Looking at the lifetimes for a 35 km displaced orbit, a mass fraction of 0.5 and a specific impulse of 3200 s shows an increase from 3.5 years for SEP control to 4.7, 9.7, 15 and 15 years for β_0 = 0.01, 0.05, 0.1 and 0.2, respectively. Similarly, the lifetime for a 150 km displaced orbit is increased from 10 months to 1.4 – 4.4 years, depending on the value for β_0. All in all, for hybrid sail control, lifetimes of 10-15 years come into reach for the smallest displacement, while reasonable lifetimes are obtained for the larger displacements.

Copyright ©2010 by Jeannette Heiligers. Published by the IAF, with permission and released to the IAF to publish in all forms.

V MASS BUDGET

The results in Fig. 3 and Fig. 8 provide the performance of both SEP and hybrid sail control in terms of propellant consumption. However, the goal of the mission is to maximize the lifetime of a spacecraft that carries a payload. It should therefore be investigated whether the mass fractions and specific impulses of Fig. 3 and Fig. 8 allow for a payload to be carried during the lifetimes shown in those figures. For this, the mass budget of the SEP and hybrid sail controlled spacecraft should be investigated. In this paper, the mass budget is based on what is proposed in Ref. [27]:

$$m_0 = m_{prop} + m_{tank} + m_{SEP} + m_P + m_{gimbal} + m_S + m_{pay} \tag{29}$$

with m_{pay} the payload mass, m_0 the initial mass, m_{prop} the propellant mass that follows from the initial mass and the mass after a certain amount of time (see Eq. (2) and Eq. (28)), $m_{tank} = 0.1 m_{prop}$ the mass of the tanks required to store the propellant and m_{SEP} the mass of the SEP thruster which is a function of the maximum power required by the SEP subsystem, $P_{SEP,\max}$, which on its own is a function of the maximum thrust required during the mission, $T_{\max}$:

$$m_{SEP} = k_{SEP} P_{SEP,\max}$$
$$P_{SEP,\max} = \frac{T_{\max} I_{sp} g_0}{2\eta_{SEP}} \tag{30}$$

with $k_{SEP} = 20$ kg/kW the specific performance of the SEP thruster and $\eta_{SEP} = 0.7$ its efficiency. Subsequently, m_P is the mass of the system that provides electrical energy to the SEP system. In case of SEP control a solar array with mass $m_P = k_{SA} P_{SEP,\max}$ is assumed with $k_{SA} = 45$ W/kg the specific performance of the solar array [29]. In case of hybrid sail control it is assumed that part of the sail is covered with thin film solar cells to provide the electrical power to the SEP system. The required area covered with solar cells can be computed from:

$$A_{TF} = \frac{P_{SEP,\max}}{W \eta_{TF}} \cos \gamma_{T_{\max}} \tag{31}$$

with $W = 1367$ W/m^2 the energy flux density of the Sun, $\eta_{TF} = 0.05$ the efficiency of the thin film and $\gamma_{T_{\max}}$ the angle between the Sun-sail line, $\hat{\mathbf{r}}_S$, and the

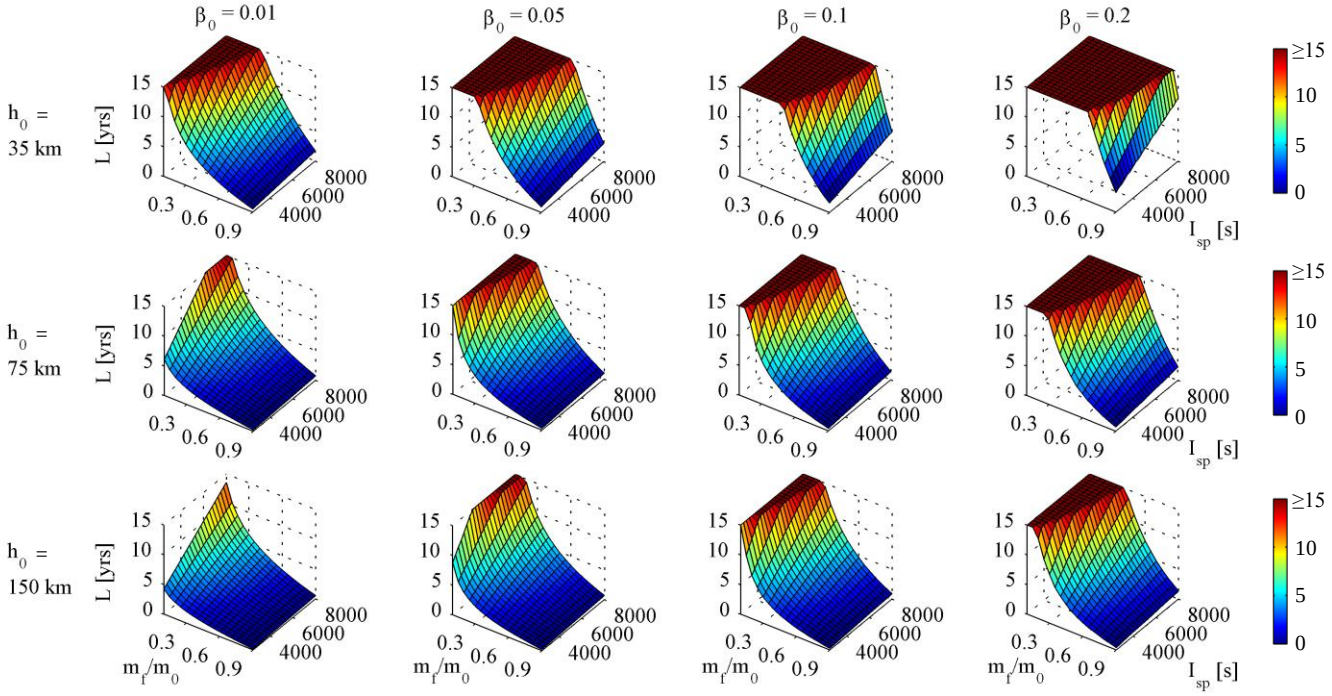

Fig. 8: Displaced geostationary orbits maintained with hybrid sail control: mission time L as a function of the specific impulse I_{sp} and the mass fraction m_f / m_0, for different values of the solar sail lightness number β_0 and the initial displacement distance h_0

Copyright ©2010 by Jeannette Heiligers. Published by the IAF, with permission and released to the IAF to publish in all forms.

solar sail acceleration vector, $\hat{\mathbf{n}}$, when $T = T_{\max}$, see also Fig. 5 and Fig. 6. From this area the mass of the thin film $m_P = \sigma_{TF} A_{TF}$ can be computed with $\sigma_{TF} =$ 100 g/m^2. Note that the influence of the thin film solar cells on the performance of the hybrid sail is neglected in this paper. Finally, $m_{gimbal} = 0.3 m_{SEP}$ is the mass of a gimbal that ensures that the solar sail and SEP thruster can steer independently from one another and m_S is the mass of the sail that can be computed through $m_S = \sigma_S A_S$ with $\sigma_S =$ 5 g/m^2 the mass per unit area of the solar sail and A_S the sail area, which is given by:

$$A_S = \frac{\beta_0 m_0}{\sigma^*} + A_{TF} \tag{32}$$

Clearly, for an SEP controlled spacecraft, both m_{gimbal} and m_S are set to zero. At a given time and for a given specific impulse, the only unknowns for computing the payload mass are the initial mass and the maximum thrust required during the mission, which are related as the initial mass is bounded by the maximum available SEP thrust, $T_{\max}$. For SEP control, this maximum thrust occurs at $t = t_0$ causing $T_{\max} = T_0$. With the required acceleration to maintain the displaced geostationary orbit given for a particular displacement distance, the maximum initial mass equals:

$$m_{0,\max} = \frac{T_0}{a} \tag{33}$$

For hybrid sail control, the maximum thrust does not necessarily occur at $t = t_0$, but can also occur in autumn (when the 'seasonal transfer' is taken into account) as shown in Fig. 7c. The resulting maximum initial masses for both SEP and hybrid sail control are shown in Fig. 9 as a function of the maximum thrust magnitude and for each of the displacement distances used so far, for different sail lightness numbers and for a specific impulse of 3200 s. Also a reference thrust magnitude of 0.2 N is indicated. The figure shows that for this reference thrust magnitude and SEP control, maximum initial masses of 1074, 501 and 251 kg are possible for displacement distances of 35, 75 and 150 km, respectively. These initial masses increase by a factor 1.05 to 2.7 for hybrid sail control, depending on the sail lightness number and the displacement distance. This is due to the reduced required SEP thrust magnitude for hybrid sails compared to pure SEP control, which was already demonstrated in Fig. 7c and mentioned as an major advantage of hybrid sail control in addition to the propellant mass savings shown in Fig. 8.

Using the maximum initial masses corresponding to a maximum thrust magnitude of 0.2 N in Fig. 9, the payload masses and lifetimes as depicted in Fig. 10 can be obtained. As a reference also the performance in terms of propellant consumption, as shown in Fig. 3 and Fig. 8, is depicted. The figure immediately shows that certain mass fractions considered in Fig. 3 and Fig. 8 do not allow for a payload mass to be carried on board the spacecraft. For example, for a 35 km displaced SEP controlled orbit and a mass fraction of 0.1 a lifetime of 12.3 years can be obtained from a propellant consumption point of view. However, looking at the corresponding payload mass, it becomes clear that this mass fraction does not allow for any payload mass, simply because the propellant mass and the mass of the tanks containing the propellant become too large. Note that the payload masses in Fig. 10 can be increased when a larger maximum thrust magnitude and therefore a larger initial mass is allowed. However, this will not increase the maximum lifetime (i.e. the time at which no payload mass remains) as all mass components scale linearly with the initial mass or equivalently with the maximum thrust magnitude. Non-zero payload masses for longer lifetimes become possible when tuning spacecraft design parameters such as k_{SEP}, η_{SEP}, k_{SA}, σ_{TF}, η_{TF} and σ_S.

Overall, Fig. 10 shows that in almost all cases hybrid sail control outperforms SEP control. Only for the largest value of β_0 the large required sail area (and with that the sail mass) becomes a disadvantage. Furthermore, the figure shows that only hybrid control allows lifetimes of current geostationary spacecraft of 10-15 years while still enabling a considerable payload to be taken onboard. For example, for a 35 km displaced orbit, a sail lightness number of 0.1 and an initial mass of 2193 kg, payload masses of 450 kg and 250 kg can be maintained in the displaced geostationary orbit for 10 and 15 years, respectively.

Although the performance for a 35 km displaced orbit is highly promising, the performance of higher displaced orbits is not. Both the lifetime and the payload mass decrease significantly when larger displacements are considered. However, the performance of these larger displacements improves significantly if an increase in the maximum thrust magnitude is allowed. To show this improvement, a maximum thrust level of 1 N is assumed, which is considered reasonable for next generation SEP systems. Subsequently, requiring a payload mass of at least 200 kg, the results in Table 1 can be found for a displacement of 150 km and a specific impulse of 3000 s. This value for the specific impulse is somewhat smaller than the value used throughout this paper in order to compensate the increase in the mass of the SEP system due to the larger value for $T_{\max}$, see Eq. (30). Table 1 shows that a payload mass of 200 kg is indeed possible for reasonable values for the initial mass. The lifetime is,

Copyright ©2010 by Jeannette Heiligers. Published by the IAF, with permission and released to the IAF to publish in all forms.

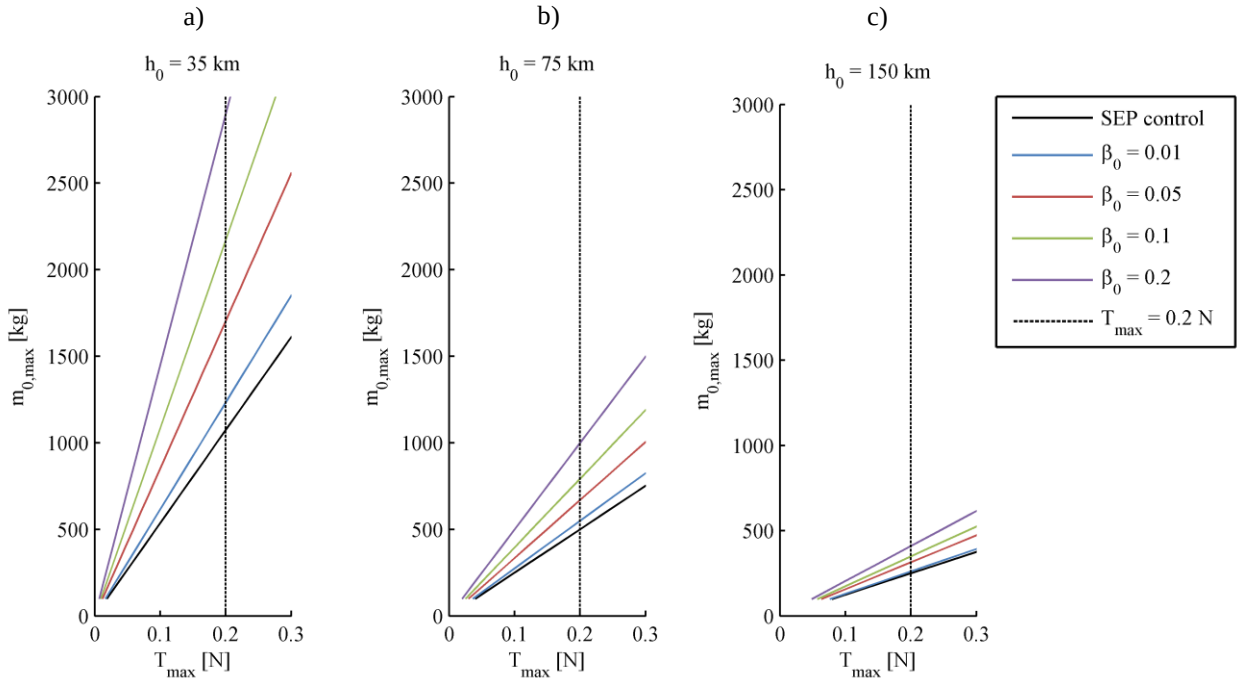

Fig. 9: Maximum initial mass as a function of the maximum thrust magnitude for different values of the displacement distance h_0 and the sail lightness number β_0 and for $I_{sp} = 3200$ s

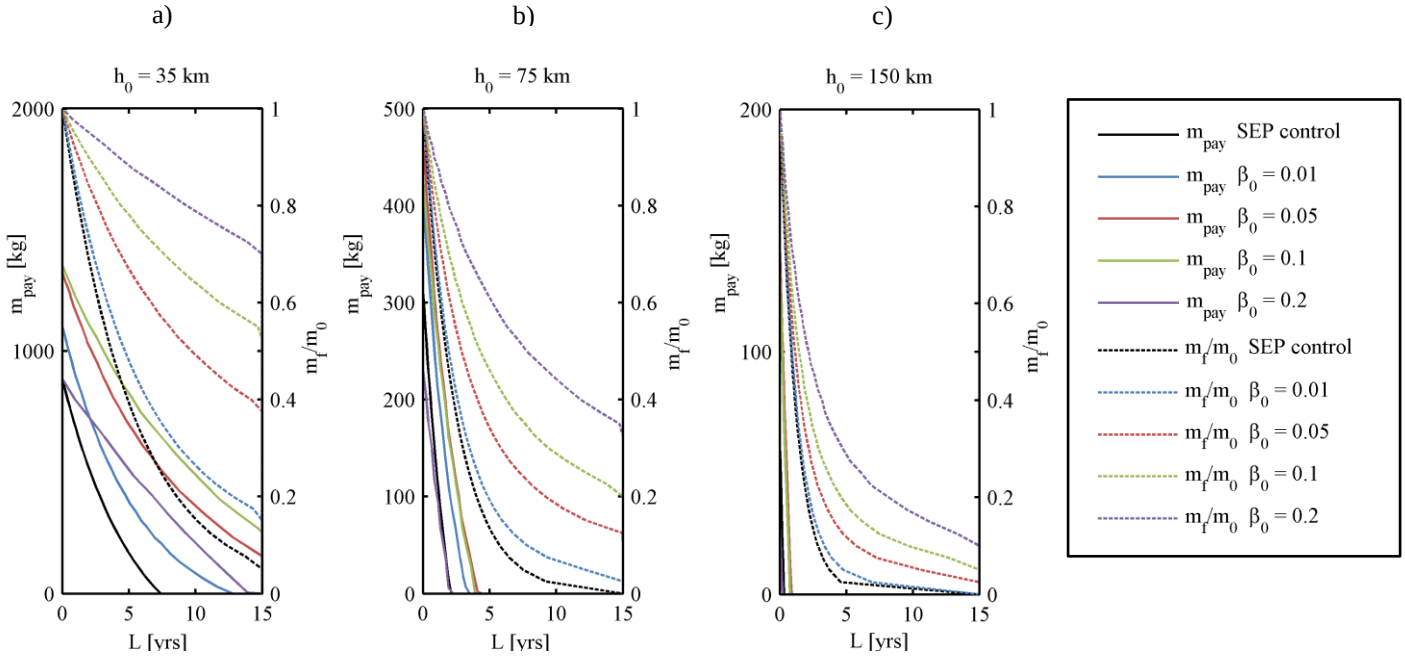

Fig. 10: Lifetime as a function of the payload mass (solid lines) and mass fraction (dashed lines) for different values of the displacement distance h_0 and the sail lightness number β_0 and for $I_{sp} = 3200$ s

Copyright ©2010 by Jeannette Heiligers. Published by the IAF, with permission and released to the IAF to publish in all forms.

however, still rather short, just over 0.5 year. It can therefore be concluded that a 150 km displaced geostationary orbit is feasible using hybrid sail control, be it for rather short periods of time. 150 km displaced geostationary orbits are therefore perfect for the concept of 'customized service' using a mobile displaced geostationary platform. Then, the displaced geostationary orbit is only maintained for a relatively short period of time to provide additional coverage when needed (e.g. during the Olympics or World Cup) and is transferred into a Keplerian parking orbit when inoperative. With only hours or days of coverage needed, the 150 km displaced geostationary orbit can transform its rather short lifetime into multiple smaller missions extended over a much longer lifetime. To show the feasibility of this concept, the next section will investigate the transfer that is required to transfer the spacecraft from and to the Keplerian parking orbit.

		$\beta_0 = 0.01$	$\beta_0 = 0.05$	$\beta_0 = 0.1$
L	[yrs]	0.55	0.59	0.52
m_{pay}	[kg]	205	201	207
$T_{\max}$	[N]	0.95	0.95	0.92
m_0	[kg]	1250	1500	1750

Table 1: Lifetime L, payload mass m_{pay} and initial mass m_0 for a 150 km displaced geostationary orbit allowing $T_{\max} \leq 1.0$ N, requiring $m_{pay} \geq 200$kg and assuming $I_{sp} = 3000$ s

VI TRANSFER ORBITS

In the previous sections two types of transfers where mentioned to improve the performance of hybrid sail control to maintain the displaced geostationary orbit. This section will investigate these transfers.

VI.I 'Seasonal transfer'

As mentioned in Section IV, the obliquity of the ecliptic causes hybrid sail control for displaced geostationary orbits to perform best when a spacecraft is displaced *above* the equatorial plane in winter and *below* the equatorial plane in summer. To accomplish this, the spacecraft will have to be transferred from above the equatorial plane to below the equatorial plane and vice versa twice per year: once in spring (above to below) and once in autumn (below to above). This section will optimize this transfer for the SEP propellant consumption, which implies solving an optimal control problem. An optimal control problem is to find a state history $\mathbf{x}(t) \in \mathbb{R}^{n_x}$ and a control history $\mathbf{u}(t) \in \mathbb{R}^{n_u}$, $t \in \left[t_0, t_f \right]$, subject to the dynamics:

$$\dot{\mathbf{x}}(t) = \mathbf{f}(\mathbf{x}(t), \mathbf{u}(t), t) \tag{34}$$

that minimize the cost function:

$$J = \varphi\left(\mathbf{x}_0, \mathbf{x}_f, t_0, t_f\right) + \int_{t_0}^{t_f} L\left(\mathbf{x}(t), \mathbf{u}(t), t\right) dt \tag{35}$$

and satisfy the constraints

$$\mathbf{c}(\mathbf{x}, \mathbf{u}, t) \leq 0 \tag{36}$$

These constraints can include event constraints on the initial and final states and time, bounds on the state variables, control variables and time and path constraints. The first term on the right hand side of Eq. (35) is the endpoint cost function, which is only a function of the initial and final states and initial and final time, while the second term is the Lagrange cost function which is a function of time. To solve this optimal control problem the open source tool PSOPT has been applied [30]. PSOPT implements a direct pseudo-spectral method to solve the optimal control problem. By discretizing the time interval into a finite number of nodes, the infinite dimensional optimal control problem is transformed into a finite dimension non-linear programming (NLP) problem. Pseudo-spectral methods use Legendre or Chebyshev polynomials to approximate and interpolate the time dependent variables at the nodes. The advantage of using pseudo-spectral methods is that the derivatives of the state functions at the nodes are computed by matrix multiplication only and that any integral associated with the problem is approximated using well known Gauss quadrature rules.

To optimize the 'seasonal transfer' for the SEP propellant consumption, the cost function equals:

$$J = -m_f \tag{37}$$

with m_f the final mass of the spacecraft. The seasonal transfer is described using a spherical reference frame $S(r, \theta, \phi)$ centred at the Earth, see Fig. 11. The in-plane angle θ is measured in counter clockwise direction from the x_S-axis that coincides with the start of the transfer (i.e. for $t = 0$, $\theta = 0$) and the out-of-plane angle ϕ is measured from the (x_S, y_S)-plane that is parallel to the equatorial plane. For an SEP controlled spacecraft the state vector at any point in the trajectory then becomes:

$$\mathbf{x} = \begin{bmatrix} r & \theta & \phi & V_r & V_\theta & V_\phi & m \end{bmatrix} \tag{38}$$

with V_r, V_θ and V_ϕ the velocity in r, θ and ϕ direction, respectively and m the mass of the spacecraft. With the transfer starting and ending in a displaced geostationary orbit the initial, $\mathbf{x}_0$, and final,

Copyright ©2010 by Jeannette Heiligers. Published by the IAF, with permission and released to the IAF to publish in all forms.

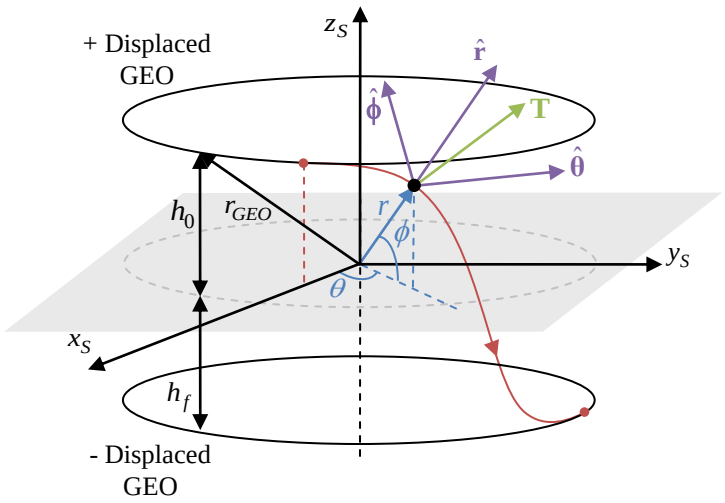

Fig. 11: Definition of spherical reference frame, control components and control angles to describe the 'seasonal transfer'

$\mathbf{x}_f$, state vectors are given by:

$$\begin{aligned}\mathbf{x}_0 &= [\, r_{GEO} \quad 0 \quad \phi_0 \quad 0 \quad \sqrt{\mu/r_{GEO}}\cos\phi_0 \quad 0 \quad m_0 \,]^T \\ \mathbf{x}_f &= [\, r_{GEO} \quad \theta_f \quad \phi_f \quad 0 \quad \sqrt{\mu/r_{GEO}}\cos\phi_f \quad 0 \quad - \,]^T\end{aligned} \tag{39}$$

with the final mass free. The final in-plane angle θ_f is restricted to:

$$\theta_f = \omega_{GEO} t_f \tag{40}$$

with ω_{GEO} the angular velocity in the (displaced) geostationary orbit to ensure that the longitude of the spacecraft in the displaced geostationary orbit is unchanged after the transfer. Furthermore, $\phi_0 = \sin^{-1}(h_0 / r_{GEO})$ and $\phi_f = \sin^{-1}(h_f / r_{GEO})$. Correct signs for h_0 and h_f will ensure correct signs for ϕ_0 and ϕ_f.

Using a two-body model the equations that describe the motion of the spacecraft in the transfer become:

$$\dot{\mathbf{x}} = \begin{pmatrix} V_r \\ V_\theta/(r\cos\phi) \\ V_\phi/r \\ V_\theta^2/r + V_\phi^2/r - \mu/r^2 + (T_r/m) \\ -V_r V_\theta/r + V_\theta V_\phi \tan\phi/r + (T_\theta/m) \\ -V_r V_\phi/r - V_\theta^2 \tan\phi/r + (T_\phi/m) \\ -T/(I_{sp} g_0) \end{pmatrix} \tag{41}$$

with $\mathbf{u} = \begin{bmatrix} T_r & T_\theta & T_\phi \end{bmatrix}$ the control vector consisting of the Cartesian components of the SEP thrust acceleration. Using Cartesian components requires the following path constraint:

$$\sqrt{T_r^2 + T_\theta^2 + T_\phi^2} \le T_{\max} \tag{42}$$

Finally, the bounds on the state and control variables and the transfer time are set to:

$$\begin{aligned} \mathbf{x}_L &= [\, R_E + 100 \quad 0 \quad -0.5\pi \quad -10 \quad -10 \quad -10 \quad 0 \,]^T \\ \mathbf{x}_U &= [\, R_E + 10000 \quad 4\pi \quad 0.5\pi \quad 10 \quad 10 \quad 10 \quad m_0 \,]^T \\ \mathbf{u}_L &= [\, -T_{\max} \quad -T_{\max} \quad -T_{\max} \,] \\ \mathbf{u}_U &= [\, T_{\max} \quad T_{\max} \quad T_{\max} \,] \\ t_L &= 0 \\ t_U &= 1 \text{ day} \end{aligned} \tag{43}$$

with R_E the radius of the Earth and $T_{\max}$ the maximum allowed thrust magnitude. Distances are provided in km, velocities in km/s and angles in radians.

PSOPT requires a first guess to initialize the optimization. To obtain this first guess, a shaped based approach is used in which the shape of the transfer is fixed and the required controls to perform that transfer are sought for. For this, the transfer is considered in a rotating reference frame that rotates with respect to an inertial frame at constant angular velocity equal to the angular velocity of the (displaced) geostationary orbit. Within this rotating frame, spacecraft in the displaced geostationary orbits are stationary. The transfer between the orbits is assumed to be the shortest path possible and a parabolic velocity profile is adopted to ensure zero velocities at the start and end of the transfer.

The results of the optimization in PSOPT are given in Table 2 with the corresponding thrust profiles in Fig. 12. A maximum thrust magnitude of 0.2 N is assumed leading to the use of the initial masses as determined in Fig. 9. To consider the worst case scenario, the initial masses corresponding to $\beta_0 = 0.2$ are selected. The table shows a relatively worse performance for smaller displacements which can be explained by the higher initial mass that can be put in the orbit without exceeding the maximum thrust level of 0.2 N while in-orbit. Table 2 furthermore shows that almost negligible amounts of propellant are needed to perform the 'seasonal transfer', which justifies the usage of this switch in Section IV to improve the performance of hybrid sail control. The reason for the extremely small amounts of propellant needed for the 'seasonal transfer' can be found in the fact that the spacecraft falls into a Keplerian orbit when switching off the thrust in the displaced geostationary orbit. The start of this Keplerian orbit coincides with the apogee, while the perigee almost touches the displaced geostationary orbit on the other side of the equatorial plane [2]. Thus, only a tiny thrust force in the form of a bang-off-bang

Copyright ©2010 by Jeannette Heiligers. Published by the IAF, with permission and released to the IAF to publish in all forms.

h_0 [km]	m_0 [kg]	m_{prop} [g]
±35	2912	2.67
±75	1020	1.05
±150	436	0.66

Table 2: Required propellant mass for optimized 'seasonal transfer'

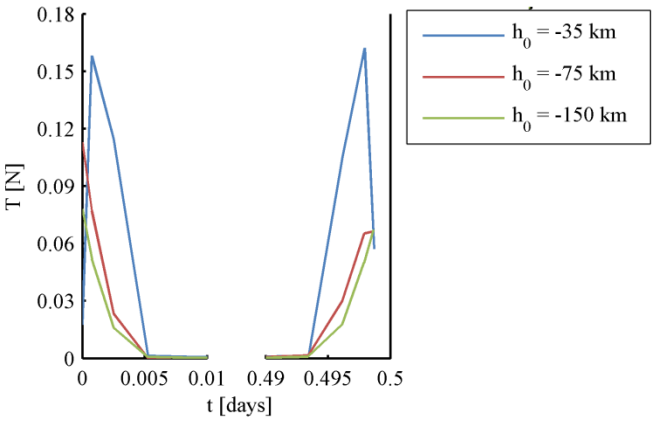

Fig. 12: Thrust profile for optimized 'seasonal transfer'

control is needed to overcome the small offset between the perigee of the Keplerian transfer orbit and the displaced geostationary orbit.

VI.II Transfer from and to parking orbit

In Section V the concept of 'customized service' by using a mobile displaced geostationary platform was introduced. Then, the spacecraft is transferred into a displaced geostationary orbit for a relatively short period of time to deliver any required coverage and is transferred back into a Keplerian parking orbit when the coverage is no longer needed. This parking orbit and the transfer that are involved in this concept are depicted in Fig. 13. The parking orbit thus lies inside the geostationary orbit where the distance between the parking orbit and the geostationary orbit equals the (absolute value of the) displacement distance. In this way, the parking orbit is as close to the displaced geostationary orbit as possible without interfering with either the geostationary or the displaced geostationary orbit.

The investigation of this transfer is very similar to the method used for the 'seasonal transfer'. The definition of the state and control variables is the same as are the equations of motion. Only the initial and final states differ. When the transfer from the parking orbit to the displaced geostationary orbit is considered, these become:

$$\mathbf{x}_0 = [r_{GEO} - |h| \quad 0 \quad 0 \quad 0 \quad \sqrt{\mu/(r_{GEO} - |h|)} \quad 0 \quad m_0]^T \quad (44)$$

$$\mathbf{x}_f = [r_{GEO} \quad - \quad \phi_f \quad 0 \quad \sqrt{\mu/r_{GEO}}\cos\phi_f \quad 0 \quad - \quad]^T \quad (45)$$

with the final in-plane angle and final mass free. Phasing between the parking orbit and the displaced geostationary orbit will have to ensure that the spacecraft is inserted into the displaced geostationary orbit at the correct longitude. Note that when the transfer from the displaced orbit to the parking orbit is considered, the initial condition equals Eq. (45) and the final condition becomes Eq. (44).

Also the optimization of the transfer is similar to the optimization of the 'seasonal transfer'. The same objective function, bounds on the state and control variables and path constraint can be applied. Even the method to generate the initial guess is the same. The only slight difference is the fact that a somewhat larger transfer time is allowed, setting the sixth equation in Eq. (43) equal to $t_U = 10$ days. The results of the optimization are shown in Table 3, Fig. 14 and Fig. 15. Although the required propellant is a factor 100 larger than for the 'seasonal transfer', it still requires only modest propellant budgets. Improvement could be made by using the solar sail in case hybrid sail control is used to maintain the displaced geostationary orbit, but this approach is not considered in this paper. The transfer itself is also shown in Fig. 14 from which it becomes clear that the final orbit (either the displaced geostationary orbit or the parking orbit) is reached by slowly increasing or decreasing the inclination of the orbit, which is achieved in an efficient way as the SEP engine thrusts only at the orbital nodes, see Fig. 15.

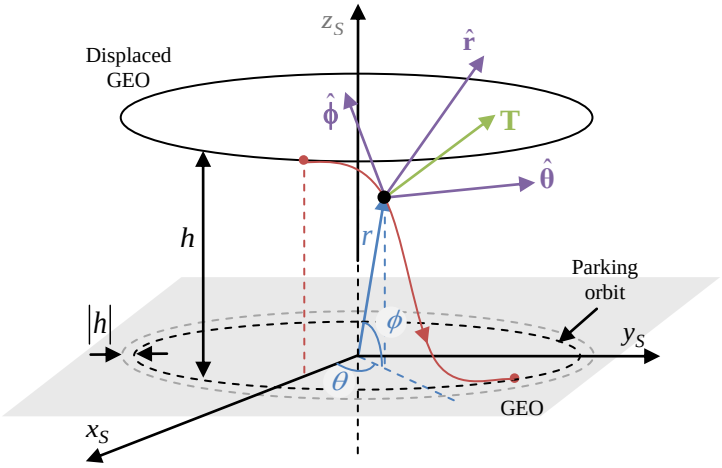

Fig. 13: Definition of parking orbit for customized geostationary service

Copyright ©2010 by Jeannette Heiligers. Published by the IAF, with permission and released to the IAF to publish in all forms.

VII CONCLUSIONS

In this paper geostationary orbits displaced above and below the equatorial plane have been proposed to increase the capacity of the geostationary ring that is starting to get congested. To maintain the orbit two types of control have been suggested, Solar Electric Propulsion (SEP) control and hybrid sail control. Both types of control have been optimized for the SEP propellant consumption, thereby maximizing the mission lifetime and/or payload mass. SEP control appeared to enable lifetimes of a few months in a 150 km displaced orbit to a few years in a 35 km displaced orbit, the minimum to rise above the geostationary station keeping box. However, investigating the spacecraft mass budget showed that only for small displacements reasonable payload masses of a few hundred kilograms could be maintained for a few years. By adding a solar sail to the SEP system, thereby creating hybrid sail control, the demand on the SEP system could be lowered significantly while enabling a mission that is impossible using only solar sailing due to the obliquity of the ecliptic. An even better performance was obtained by alternating the displacement between above (autumn – spring) and below (spring – autumn) the equatorial plane during the year to use the solar sail to its full potential, introducing a so-called 'seasonal transfer'. Optimizing this transfer for the SEP propellant consumption showed that this transfer comes almost for free. Employing this transfer showed that hybrid sail control outperforms the pure SEP case both in terms of payload capacity and mission lifetime for all displacements considered. Hybrid sail control provided lifetimes of 10-15 years (equal to current geostationary missions) for a 35 km displaced orbit and for considerable payload masses of 250 – 450 kg. Allowing a somewhat larger maximum thrust magnitude also resulted in reasonable payload masses of 200 kg for the higher displaced orbits, be it for relatively short periods of time. These orbits therefore appeared to be especially useful for the concept of 'customized service' in which the spacecraft is only put into the displaced orbit for relatively short periods of time (hours or days) to provide coverage when needed. When not operational, the spacecraft is transferred into a Keplerian parking orbit. Optimizing this transfer showed that only a modest propellant budget of approximately 200 g is required.

ACKNOWLEDGMENTS

This work was funded by the European Research Council Advanced Investigator Grant - 227571: Visionary Space Systems: Orbital Dynamics at Extremes of Spacecraft Length-Scale. The author would like to thank the supervisors of this work, Dr. Colin R. McInnes, Dr James D. Biggs and Dr Matteo Ceriotti for their valuable input and feedback. Finally, the author thanks Dr. Victor M. Beccera for providing the software tool PSOPT freely and for providing advice on its use.

a)

h_f [km]	m_0 [kg]	m_{prop} [kg]
±35	2912	0.269
±75	1020	0.204
±150	436	0.171

b)

h_0 [km]	m_0 [kg]	m_{prop} [kg]
±35	2912	0.292
±75	1020	0.209
±150	436	0.176

Table 3: Required propellant mass. a) Transfer from parking orbit to displaced geostationary orbit. b) Transfer from displaced geostationary orbit to parking orbit.

a) b)

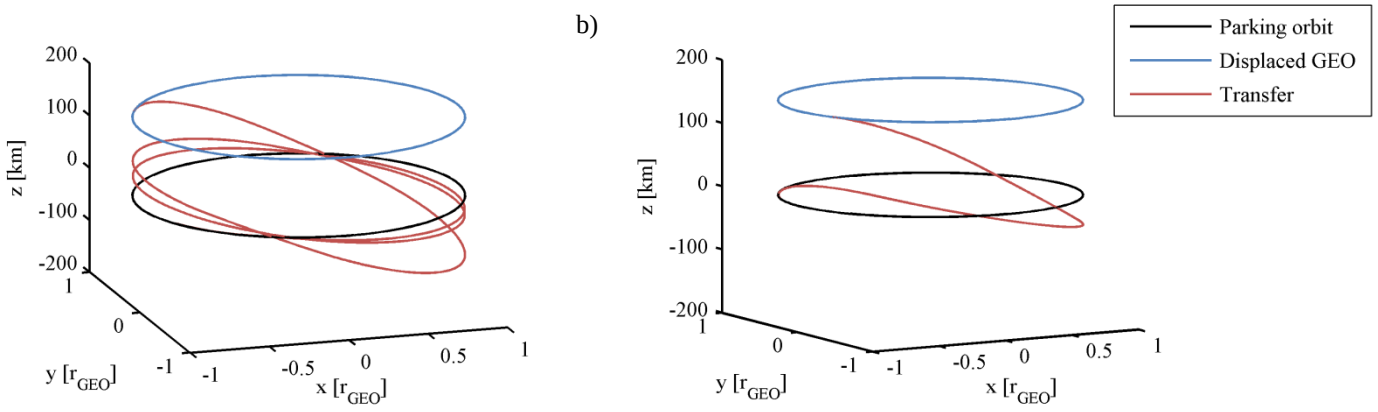

Fig. 14: Transfer for a 150 km displaced geostationary orbit. a) Transfer from parking orbit to displaced geostationary orbit. b) Transfer from displaced geostationary orbit to parking orbit.

Copyright ©2010 by Jeannette Heiligers. Published by the IAF, with permission and released to the IAF to publish in all forms.

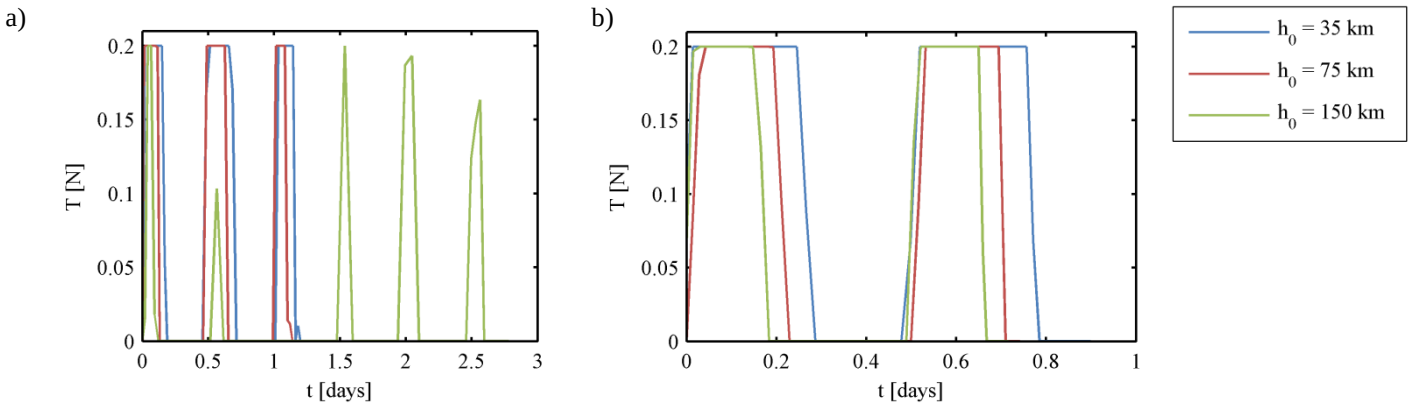

Fig. 15: Thrust profile for 35, 75 and 150 km displaced orbits. a) Transfer from parking orbit to displaced geostationary orbit. b) Transfer from displaced geostationary orbit to parking orbit.

REFERENCES

1. R. Jehn, A. Rossi, T. Flohrer, D. Navarro-Reyes, "Reorbiting of satellites in high altitudes", in *Proceedings of 5th European Conference on Space Debris*, Darmstadt, Germany, 2009.
2. C. R. McInnes, "Solar Sailing: Technology; Dynamics and Mission Applications", Springer-Praxis Books in Astronautical Engineering, Springer-Verlag, Berlin, 1999.
3. C. R. McInnes, "Dynamics, Stability, and Control of Displaced Non-Keplerian Orbits", *Journal of Guidance, Control, and Dynamics*, vol. 21, n. 5, p. 799-805, 1998.
4. J. D. Biggs, C. R. McInnes, T. Waters, "Control of Solar Sail Periodic Orbits in the Elliptic Three-Body Problem", *Journal of Guidance, Control, and Dynamics*, vol. 32, n. 1, p. 318-320, 2009.
5. C. R. McInnes, "The Existence And Stability Of Families Of Displaced Two-Body Orbits", *Celestial Mechanics and Dynamical Astronomy*, vol. 67, p. 167-180, 1997.
6. T. R. Spilker, "Saturn Ring Observer", *Acta Astronautica*, vol. 52, p. 259-265, 2003.
7. T. J. Waters, C. R. McInnes, "Periodic Orbits Above the Ecliptic in the Solar-Sail Restricted Three-Body Problem", *Journal of Guidance, Control, and Dynamics*, vol. 30, n. 3, p. 687-693, 2007.
8. J. Simo, C. R. McInnes, "Solar Sail Orbits at the Earth-Moon Libration Points", *Communications in Nonlinear Science and Numerical Simulation*, vol. 14, n. 12, p. 4191-4196, 2009.
9. D. J. Grebow, M. T. Ozimek, K. C. Howell, "Advanced Modeling of Optimal Low-Thrust Lunar Pole-Sitter Trajectories", *60th International Astronautical Congress*, Daejon, South Korea, 2009.
10. J. Bookless, C. R. McInnes, "Dynamics and Control of Displaced Periodic Orbits Using Solar-Sail Propulsion", *Journal of Guidance, Control, and Dynamics*, vol. 29, n. 3, p. 527-537, 2006.
11. JAXA, "Press Releases: Small Solar Power Sail Demonstrator 'IKAROS' Confirmation of Photon Acceleration", available from: http://www.jaxa.jp/press/2010/07/20100709_ikaros_e.html, cited 1 September 2010.
12. M. Macdonald, C. R. McInnes, "Solar Sail Mission Applications and Future Advancement", *2nd International Symposium on Solar Sailing*, New York, USA, 2010.
13. S. Baig, C. R. McInnes, "Light Levitated Geostationary Cylindrical Orbits are Feasible", *Journal of Guidance, Control, and Dynamics*, vol. 33, n. 3, p. 782-793, 2010.
14. R. McKay, M. Macdonald, F. Bosquillon de Frescheville, M. Vasile, C. McInnes, J. Biggs, "Non-Keplerian Orbits Using Low Thrust, High ISP Propulsion Systems", *60th International Astronautical Congress*, Daejeon, South Korea, 2009.
15. M. D. Rayman, P. A. Chadbourne, J. S. Culwell, S. N. Williams, "Mission Design for Deep Space 1: A Low-Thrust Technology Validation Mission", *Acta Astronautica*, vol. 45, p. 381-388, 1999.
16. G. D. Racca, A. Marini, L. Stagnaro, J. van Dooren, L. di Napoli, B. H. Foing, R. Lumb, J. Volp, J. Brinkmann, R. Grünagel, D. Estublier, R. Tremolizzo, M. McKay, O. Camino, J. Schoemaekers, M. Hechler, M. Khan, P. Rathsman, G. Andersson, K. Anflo, S. Berge, P. Bodin, A. Edfors, A. Hussain, J. Kugelberg, N. Larsson, B. Ljung, L. Meijer, A. Mörtsell, T. Nordebäck, S. Persson, F. Sjöberg, "SMART-1 mission description and development status", *Planetary and Space Sciences*, vol. 50, p. 1323-1337, 2002.
17. J. R. Brophy, M. A. Etters, J. Gates, C. E. Garner, M. Klatte, C. J. Lo, M. G. Marcucci, S. Mikes, G.

Copyright ©2010 by Jeannette Heiligers. Published by the IAF, with permission and released to the IAF to publish in all forms.

Pixler, B. Nakazono, "Development and Testing of the Dawn Ion Propulsion System", *42nd AIAA/ASME/SAE/ASEE Joint Propulsion Conference & Exhibit*, Sacramento, USA, 2006.

18. G. Mengali, A. A. Quarta, "Trajectory Design with Hybrid Low-Thrust Propulsion System", *Journal of Guidance, Control, and Dynamics*, vol. 30, n. 2, p. 419-426, 2007.
19. G. Mengali, A. A. Quarta, "Tradeoff Performance of Hybrid Low-Thrust Propulsion System", *Journal of Spacecraft and Rockets*, vol. 44, n. 6, p. 1263-1270, 2007.
20. J. Simo, C. R. McInnes, "Designing displaced lunar orbits using low-thrust propulsion", *Journal of Guidance, Control, and Dynamics*, vol. 33, n. 1, p. 259-265, 2010.
21. S. Baig, C. R. McInnes, "Artificial Three-Body Equilibria for Hybrid Low-Thrust Propulsion", *Journal of Guidance, Control, and Dynamics*, vol. 31, n. 6, p. 1644-1655, 2008.
22. R. J. McKay, M. Macdonald, M. Vasile, F. Bosquillon de Frescheville, "A Novel Interplanetary Communications Relay", *AIAA/AAS Astrodynamics Specialist Conference*, Toronto, Canada, 2010.
23. M. Ceriotti, C. R. McInnes, "An Earth Pole-Sitter Using Hybrid Propulsion", *AIAA/AAS Astrodynamics Specialists Conference*, Toronto, Canada, 2010.
24. B. G. Evans, "Satellite Communication Systems", 3rd edition, The Institution of Electrical Engineers, London, UK, 1999.
25. UNCOPUOS, "Long-term sustainability of outer space activities, Preliminary reflections", *47th session of the United Nations Committee on the Peaceful Uses of Outer Space (UNCOPUOS) Scientific and Technical Subcommittee*, Vienna, Austria, 2010.
26. H. Kuninaka, K. Nishiyama, I. Funaki, T. Yamada, Y. Shimizu, J. Kawaguchi, "Powered Flight of Electron Cyclotron Resonance Ion Engines on Hayabusa Explorer", *Journal of Propulsion and Power*, vol. 23, n. 3, 2007.
27. M. Ceriotti, C. McInnes, "A Near Term Pole-Sitter Using Hybrid Solar Sail Propulsion", *2nd International Symposium on Solar Sailing*, New York, USA, 2010.
28. A. Schneider, W. Sun, H. Schuff, "The European Platform LUXOR for Small Communications Satellites", *26th International Communications Satellite Systems Conference (ICSSC)*, San Diego, USA, 2008.
29. J. R. Wertz, W. J. Larson, "Space Mission Analysis and Design", 3rd edition, Microcosm Press & Kluwer Academic Publishers, 1999.
30. V. M. Becerra, "PSOPT", available from: http://www.psopt.org/.